Large-scale, proteinaceous nanotube arrays with

programmable hydrophobicity, oleophilicity and gas

permeability

Hui Sun, Benedetto Marelli*

Department of Civil and Environmental Engineering

Massachusetts Institute of Technology

Cambridge, MA 02139, USA

*E-mail: bmarelli@mit.edu

KEYWORDS: silk, nanotubes, nanopillars, templated assembly, anti-fouling, oil extraction, gas

barrier

ABSTRACT:

Nanotubular structures possess remarkable advantages in a broad range of areas, such as catalysis,

sensing, microencapsulation, selective mass transport, filtration and drug delivery. While the fields

of carbon nanotubes and nanotubes made of several non-carbon materials (e.g., metals, oxides,

semiconductors) have been progressing rapidly, proteinaceous nanotubes remained largely

underexplored. Here, by retrofitting a template wetting approach with multiple silk-based

suspensions, we present a rapidly scalable and robust technology for fabricating large arrays (e.g.

20 × 20 cm²) of well-aligned 1D nanostructures made of silk proteins. Benefitting from the

polymorphic nature of silk, precise control over the size, density, aspect ratio, and morphology

(tubes versus pillars) of silk nanostructures are achieved, which then allows for programmable

modulation of the end materials' functions and properties (e.g., hydrophobicity, oleophilicity and

1

gas permeability). The silk nanotube arrays fabricated present great utility as anti-fouling coatings against marine algae and in oil extraction from oil-water mixtures.

TEXT

Since the groundbreaking discovery of carbon nanotubes in 1991,¹ hollow nanostructures have been attracting a lot of interest in materials science and nanotechnology. Nanotubular material formats offer considerable advantages in many cases, provided by increased specific surface areas for catalysis and sensing applications,² presence of nano-/microcavities for encapsulation and compartmentalization purposes,³ and versatile design in large arrays to generate nanostructured membranes,^{4,5} among others. Besides carbon, nanotubes made of metals (e.g. Au, Ag, Pt, Pd),⁶ oxides (e.g. Fe₂O₃, Co₃O₄, TiO₂, SiO₂),⁷ semiconductors (e.g. GaN, GaAs, BN)⁸ and polymers (e.g. polystyrene, PMMA and peptides)^{9–11} have also been increasingly pursued to impact a broad range of fields such as high-performance composites, energy storage units, transistors, supercapacitors, sensors, membranes for selective gas transport, filtration, artificial muscles, and drug delivery. Nonetheless, the fabrication of nanotubular objects and more importantly their organization into macroscopic (at least centimeter scale) arrays is still a nontrivial task, especially for soft polymeric materials that are more appropriate to work at the biotic/abiotic interface.

To fabricate polymeric nanotubes, two fundamental strategies have been pursued – self-assembly and employment of sacrificial templates. While self-assembly is an effortless and elegant approach to form nanostructured objects, only a limited spectrum of materials (e.g. lipids, naturally occurring or engineered peptides, and amphiphiles) self-organize into tubular nanostructures. The dimensions of self-assembled nanotubes are also not easily adjustable in most cases. These restrictions, however, generally do not apply to template-based synthesis. In this domain, the template wetting approach first introduced by Steinhart et al. in 2002 serves as a simple and smart approach that allows for fabrication of large quantities of polymeric nanotubes through wetting of ordered porous templates (e.g. anodic aluminum oxide and macroporous silicon) by solutions or melts of a broad spectrum of polymers. Later, nanoporous polycarbonate membranes (of pore sizes 400 nm – 1 μ m) were used as templates in combination with layer-by-layer assembly to fabricate nanotubes made of structural proteins, e.g. *Dosidicus gigas* sucker ring teeth (SRT)

proteins^{16,17} and human serum albumin (HSA).^{18,19} While these studies serve as excellent proof-of-concepts to showcase the potential of template-based synthesis for producing biopolymeric nanotubes, they also have limitations particularly in their capabilities to diversify the nanostructure's morphology beyond tubular forms, due to constraints on material polymorphism and compatibility with a variety of solvent systems. Further, the design and application of proteinaceous nanoforests in the Ag/Food and environmental domains remain largely unexplored, as compared to in biomedicine.

Inspired by the previous work on using templates to guide materials assembly and motivated by the compelling need to find circular, non-toxic and biodegradable alternatives to synthetic polymers, non-renewable semiconductors and metal alloys, we developed a rapidly scalable approach for fabricating centimeter-scale arrays of well-aligned 1D nanostructures (i.e. nanotubes and nanopillars) made of silk proteins. The general silk nanotube/pillar fabrication procedure is shown in Figure 1a, where commercially available polycarbonate (PC) membranes were used as nanoporous templates for silk nanotubes/pillars fabrication. The choice of PC membranes is based on their availability in a wide range of pore sizes from several microns down to 10 nm, at a much lower cost compared to other commonly used nanoporous templates (i.e., anodic aluminum oxide and macroporous silicon) and the good wettability of their PVP-coated pore walls by silk-based solutions. As reported by previous studies, wetting of the pore walls of a nanoporous template can occur via either formation of a mesoscopic precursor liquid film or complete filling of the pore interior, depending on the surface energies of both the liquid and the pore wall. 12 Based on this principle, we designed several silk formulations to regulate the wetting and dehydration dynamics, so that different morphologies of the silk nanostructures can be achieved in the end. It was found that both silk-water suspension and silk suspended in formic acid (FA) infiltrate the PC pores through formation of a thin liquid film around the pore walls (Figure 1a,i), generating tubular structures after solvent evaporation. We speculate that this is because the adhesive forces between silk solution and the pore walls (which drive the spreading) are much stronger than the cohesive forces between silk molecules away from the pore walls (i.e. in the bulk). 9,12 Therefore, complete filling of the pore interior occurs on a much slower time scale than precursor liquid film spreading followed by solvent evaporation. With the silk nanotubes obtained (Figure 1b,i), inorganics (e.g. CaCO₃) crystallization can be pursued in the confined cylindrical pores (Figure 1b,ii), generating silk-CaCO₃ composites with the capability to regulate the phase composition of CaCO₃ (i.e. calcite and vaterite) (Figure S1), as silk is known to interact with amorphous calcium carbonate and template their crystallization.²⁰ Besides inorganic crystals, biomolecules such as enzymes could also be conveniently loaded in the silk nanotube arrays for enhanced preservation of the biomolecules' functions. To achieve this, the initial silk solution was doped with carbonic anhydrase (CAn) to generate silk-CAn nanotubes. After 12 hours of storage at 50 °C, the CAn encapsulated in silk nanotubes retained 88.5% of its initial activity (Figure S2), compared to free CAn which lost over 90% of activity at 50 °C within one hour.²¹

In order to obtain silk nanopillars, complete filling of the PC pore volume is required (Figure 1a,ii). This was achieved by adjusting the formulations of silk suspensions to be infiltrated, which resulted in different morphologies of silk nanopillars (Figure 1b, iii-v). In the first method, porous PC templates were infiltrated with a freshly prepared mixture of silk proteins, horseradish peroxidase (HRP) and hydrogen peroxide (H2O2), then incubated in a humid environment (99% RH) to prevent water evaporation, allowing sufficient time for the silk solution to fill up the entire pore volume and at the same time undergo sol-gel transition catalyzed by HRP in the presence of H₂O₂ within the PC pores.²² Successive dehydration of the silk gel-PC composite at increasing concentrations of ethanol followed by critical point drying 23 and removal of the PC template in dichloromethane (DCM) generated porous silk pillars (Figure 1b,iii). The second method to obtain silk pillars employs a silk suspension prepared by dissolving degummed silk fibers in FA and CaCl₂.²⁴ The presence of sufficient amounts of CaCl₂ in the silk suspension was found to be the key for complete liquid filling of the PC pores and generation of silk pillar structures (Figure 1b,ivv), as the highly hygroscopic nature of CaCl₂ helps retain a large amount of bound water in the silk constructs (Figure S3). More interestingly, besides the regular pillar structure obtained without any post-treatment (Figure 1b,iv), mushroom-shaped pillars (Figure 1b, v) were obtained by exposing the silk/CaCl₂-PC composites to vapors of a 80 v/v% EtOH/water solution for 3 hours followed by PC removal in DCM. Incubating the same silk/CaCl₂-PC composites in pure water vapors, however, converted the pillars to tubes (Figure S4). To the best of our knowledge, this type of versatile control over the morphologies of nanostructures made of a single biopolymer has never been achieved before.

Another important merit of using the template-based approach is that the size of silk nanotube/pillar arrays fabricated can be extremely large, which in theory only depends on the size of the porous template available. Here, a free-standing silk nanotube array of size 20 cm × 20 cm

is demonstrated as an example (Figure 1c). Large arrays of silk nanopillars can be obtained in the same way by infiltrating PC templates with the silk/CaCl₂/FA suspension followed by PC removal (Figure 1d). By using PC templates with different pore sizes (from 2 µm down to 10 nm), silk nanotubes of corresponding diameters and aspect ratios were obtained (Figure 1e,f; Figure S5, S10). Since the thicknesses of all PC templates used in this study are in the range of 6-10 µm while their pore sizes differ 3 orders of magnitude, the aspect ratios (defined by tube length divided by tube diameter) of silk nanotubes obtained range from 5 to 600. As the aspect ratio of silk nanotubes becomes larger (i.e. individual silk nanotubes become more slender), collapsing and/or aggregating of neighboring nanotubes tend to happen more easily when the silk array is air dried after being immersed in DCM to remove the PC template. To better maintain the vertical alignment of silk nanostructures, critical point drying can be used to mitigate surface tension-induced structural collapse when changing from liquid to gas phases. 16 With critical point drying, vertically aligned silk nanotubes of diameter as small as 100 nm and aspect ratio as high as 60 can be obtained (Figure 1f), which is 28 times the maximum aspect ratios achieved in nanopatterning of silk with electron and/or ion beam lithography.^{25,26} Besides the morphology and dimensions of silk nanostructures, another parameter that can be easily regulated is the molecular conformation of silk, from amorphous to different levels of crystallinity (i.e. β-sheet contents) (Figure 1g). For example, annealing of amorphous silk nanoarrays in water vapor or vapor from 80 v/v% EtOH/water can generate silk nanoarrays made of type II β-turns and antiparallel β-pleated sheets, respectively.²⁷ Other silk polymorphs can also be introduced through templated crystallization of silk on peptide seeds, e.g. a dodecapeptide (GAGSGA)₂ and a coiled-coil peptide (referred to as HBSP) derived from honeybee silk AmelF3. These two peptides are known to interact with amorphous silk molecules and drive their folding and assembly into ordered conformations that resemble those of the peptide seeds.²⁸

Considering that the silk nanotube arrays possess well-aligned sub-micron features and a large pore volume at the surface, which are known to entrap air pockets in between water droplets and the underlying substrate, ^{29,30} we investigated the hydrophobicity of the silk nanotube arrays. In particular, contact angles (CA) of water droplets were measured on three types of nanotube arrays made of (1) silk dried from silk-FA suspension; (2) silk annealed in 80 v/v% EtOH/water vapor; and (3) silk annealed in water vapor (Figure 2a). We first characterized the intrinsic hydrophobicity of bulk silk material without the effects of nanostructures, and found that the silk dried from a silk-

FA suspension is slightly hydrophobic with a CA of $100.0 \pm 0.4^{\circ}$, while both 80% EtOH-annealed and water-annealed silk are hydrophilic with a CA of $76.7 \pm 1.3^{\circ}$ and $58.0 \pm 1.3^{\circ}$, respectively. This indicates that the three silk materials possess different surface energy, presumably because the silk chains are folded and assembled differently (i.e. having different polymorphs) (Figure 1g). Contact angles of silk nanotube arrays with different tube diameter ϕ and density (represented by an average inter-tube distance d) were then measured for all three silk materials, which showed near superhydrophobicity with water CAs in the range of 134-138° for all silk-FA nanotubes of $\phi \le 1 \mu m$. Even for the nanotube arrays made from 80% EtOH-annealed and water-annealed silk, which are intrinsically hydrophilic, they show good hydrophobicity with CAs in the range of 121-127° in the case of ϕ , d = 1, 2.2 and 0.6, 1.8 μm .

In light of the high water repellency and the micro-/nanostructured surface features of nanotube arrays made from silk-FA suspension, we further hypothesized that they might function as antifouling coatings against microorganisms when submerged under water. ^{31–33} To test this hypothesis, we chose a species of marine algae named *porphyridium cruentum*, which has a spherical shape of around 4 µm in diameter (Figure S6). The choice of this particular alga was based on its extremely high fouling capability on common substrates like glass within a few hours and the fact that it produces a red protein-pigment complex so that we can easily measure algae coverage over the silk nanotube array through fluorescence microscopy.³⁴ Here, our testing samples were glass coverslips coated with silk nanotube arrays of different tube diameter ϕ and inter-tube distance d. PEG-coated glass coverslips were used as positive control, as PEG is a well-known coating material to inhibit non-specific binding from proteins and microorganisms.³⁵ Additionally, bare glass coverslips were included as negative control. We incubated the samples and controls in porphyridium culture for 7 days, and measured algae coverage (red areas) every 24 hours from their fluorescence microscopy images (Figure 2b,c). Compared to bare glass on which algae growth started off right away (Figure S7), both PEG-coated and silk nanotube-coated surfaces showed a lagging period during which algae fouling remained at a very low level (Figure 2b). The length of the lagging period, however, varies depending on the geometric parameters (ϕ, d) of the nanotube array. Regardless of their tube diameters and densities, all silk nanotube arrays showed less fouling than the positive control (Figure 2b). Among the silk nanotube arrays tested, the array of ϕ , d = 2, 7.1 µm displayed the highest algae fouling, due to the fact that the average inter-tube distance in this case is larger than the size of individual alga, thereby the algae can easily occupy

the inter-tube spaces once the liquid meniscus hanging over the nanotubes collapse. The other low-performing nanotube array was the one of ϕ , d=200, 600 nm, where we speculate that the individual nanotubes were too slender to withstand the perturbations exerted by algae attachment, which caused the silk array to gradually lose its original forest-like morphology and water-repellency over time. Based on these results, we can see that the initial hydrophobicity of the silk nanotube arrays is compromised over time, due to the dynamic algae-nanotube interactions that come from algae adhesion and anchoring. We argue that there is a trade-off in nanotube design for anti-fouling performance, where the nanotubes should be sufficiently small in diameter and densely packed which imparts a high initial hydrophobicity, and at the same time not too slender (i.e. having a relatively small aspect ratio) to ensure longevity of water-repellency by maintaining nanotube stability against various disruptive forces. Agreeing with this rule of thumb, our results show that the silk nanotube array with a medium tube diameter, inter-tube distance and aspect ratio (namely, ϕ , d, $\rho = 400$ nm, 800 nm, 25) possesses the best anti-fouling performance with minimal algae fouling over the entire period of study (Figure 2b,c).

Besides water, another type of liquid that is of substantial interest in wettability studies is oil. As the surface tension of water (i.e., 72 mN·m⁻¹) is usually much larger than that of oil (typically around 30 mN·m⁻¹), when the surface energy of a solid substrate lies between those of water and oil, it will possess simultaneous hydrophobicity and oleophilicity.³⁶ Further, proper design of material micro-/nanostructures can be employed to tune surface properties towards superhydrophobicity and superoleophilicity. Silk fibroin from Bombyx mori cocoons in its original fiber format has a surface energy of 43 mN·m⁻¹, ³⁷ thereby having the potential to be fabricated as a water-repellent and oil-absorbing material.³⁸ Here, we chose dibutyl adipate (DA, surface tension = 31.2 mN·m⁻¹ at 22 °C) as a model oil to characterize the wettability of silk nanotube arrays by general oily compounds. The choice of DA was based on its wide usage in agriculture, food and cosmetics industry (e.g. as a solvent for many pesticides/herbicides/fungicides). CA measurements showed that wetting of the silk nanotube arrays by DA starts with a low CA (in the range of 10-25°) which then drops quickly to 0° within 10-30 seconds (Figure 3a; Movie S1). This is resulted from fast spreading and penetrating of DA across the silk nanotube arrays due to their porous nature. Albeit being superoleophilic in all cases, the initial CA values (Figure 3b) and CA change rates (Figure 3c) show obvious differences depending on the nanotube arrays' geometric configurations. Complete oil penetration in the silk nanotube array was also verified by depositing

an oil droplet that has a refractive index (RI = 1.55) very similar to that of silk,³⁹ which turned the nanoarray's original white appearance into transparent (Figure 3d).

Based on the fact that the silk nanotube arrays are both near superhydrophobic and superoleophilic, we then evaluated their efficacy in extracting oil from oil-water mixtures.^{40,41} To this end, DA dyed with Sudan III was vigorously mixed with water to form a homogenous emulsion. Upon adding an emulsion droplet on a silk nanotube array, the oil component spread quickly over the entire nanostructured silk array, leaving only a clear water droplet on top of the array in the end (Figure 3e; Movie S2). Importantly, oil spreading was confined only within the nanotubular region of the membrane and did not extend into bulk silk, indicating that the nanotubular structure of the silk array plays a pivotal role in superoleophilicity and oil extraction. Indeed, when the same DA-water emulsion was deposited on bulk silk films, no extraction of DA in the bulk film was observed (Figure S8). Further characterization revealed that the oil extraction by silk nanotube arrays follows a random walk model characterized by equation $x = \sqrt{D \cdot t}$ (where D represents the diffusion coefficient), 42 and the oil diffusion coefficient varies depending on the geometric configuration (\phi, d) of nanotube arrays (Figure 3f). Additionally, as the nanotubes become more slender ($\phi < 1 \mu m$) and more densely packed, they tend to collapse and aggregate at their open ends, forming ridges of nanotubes (Figure S9), in contrast to the well-isolated nanotubes of ϕ , d= 2, 7.1 μ m and 1, 2.2 μ m (Figure 1c; Figure S5a). These differences in microscopic morphologies give rise to isotropic and anisotropic oil diffusion observed in nanotube arrays of ϕ ≥ 1 µm and $\phi < 1$ µm, respectively (Figure 3f, g). Diffusion coefficients for each nanotube configuration (n=3) were plotted in Figure 3h for easier comparison, from which an anisotropy index (defined by $D_{\text{max}}/D_{\text{min}}$) was also calculated (Figure 3i), showing that arrays with more slender and more densely packed nanotubes exhibit larger anisotropy in oil extraction.

Finally, we studied gas transport through the silk nanotube membranes, which is an important property to consider when applying such materials for food and biomedical applications. ^{43,44} Among the gases of interest, we started with water vapor and measured water vapor permeability (WVP) of the silk nanotube membranes. Interestingly, we found that nanostructured silk membranes show lower WVP compared to bulk silk membranes of the same thickness (Figure 4a), and that the decrease of WVP presents a linear relationship with respect to the logarithm of the nominal pore size (NPS) of the nanostructured silk membrane (Figure 4b). It is speculated that the

improved water vapor barrier property might derive from a combination of higher hydrophobicity possessed by the nanotube arrays, together with an increasing hinderance to water vapor mobility through enhanced silk-water vapor interaction due to larger specific surface area present in the nanostructured array with smaller NPS. 45 Despite an apparent linear relationship between WVP and log NPS observed, it is important to note that NPS alone does not fully capture the complex pore geometry of the nanostructed silk membranes. For example, SEM analysis of silk membranes fabricated from PC templates of 10 nm pores depicts a complicated morphology with hierarchical pore structures spanning 3 orders of magnitude, i.e. having micron-scale larger pores and entangled silk nanowires inside the micrometer pores (Figure S10), whereas silk membranes fabricated from PC templates of larger pore sizes present a more uniform nanotubular structure (Figure 1e,f; Figure S5b-d). To demonstrate application of the silk nanotube membranes on objects with complicated surface topography (e.g. food), a free-standing and highly flexible silk nanotube membrane was conformably wrapped around a strawberry as a coating/packaging material (Figure 4c).

In conclusion, we report a simple yet robust approach for fabricating large arrays of well-aligned 1D nanostructures made of silk proteins, through confined assembly of silk within nanoporous templates. By regulating the biopolymer formulation thereby changing its surface energy, wetting of the nanoporous templates occur via either formation of a mesoscopic liquid film or complete filling of the pore interior, generating large arrays ($20 \times 20 \text{ cm}^2$) of well-aligned silk nanotubes or nanopillars, respectively. Such silk nanotube/pillar arrays can either be grown directly on an external substrate as a coating material or be fabricated as a free-standing membrane, which are found to be both highly hydrophobic and superoleophilic. Benefiting from its high waterrepellency, substrates coated with silk nanotube arrays present significantly reduced fouling by marine algae, compared to commercially available anti-fouling coatings. Furthermore, the silk nanotube arrays can rapidly extract oil from oil-water emulsions due to its simultaneous hydrophobicity and superoleophilicity, which could have important applications in oil spill response, lipid-water separation for food applications, and encapsulation of oil-soluble agrochemicals for crop protection. Lastly, the nanostructured silk membranes are found to possess lower water vapor permeability than bulk membranes, which may enable their use as a more effective material for food packaging. Together, these results demonstrate that by integrating the template wetting approach with the versatility of silk proteins, precise control over the size, density, aspect ratio, morphology and polymorphs of silk nanostructures can be achieved, which

then allows for programmably regulating the functions and macroscopic properties of the end materials. We believe that the biodegradable, non-toxic and edible nature of silk proteins in combination with the capability to organize silk proteins into centimeter-scale arrays with well-aligned nanostructures of customized morphologies will open up exciting opportunities in a broad range of fields, from AgroFood and biomedicine to the built environment.

FIGURES

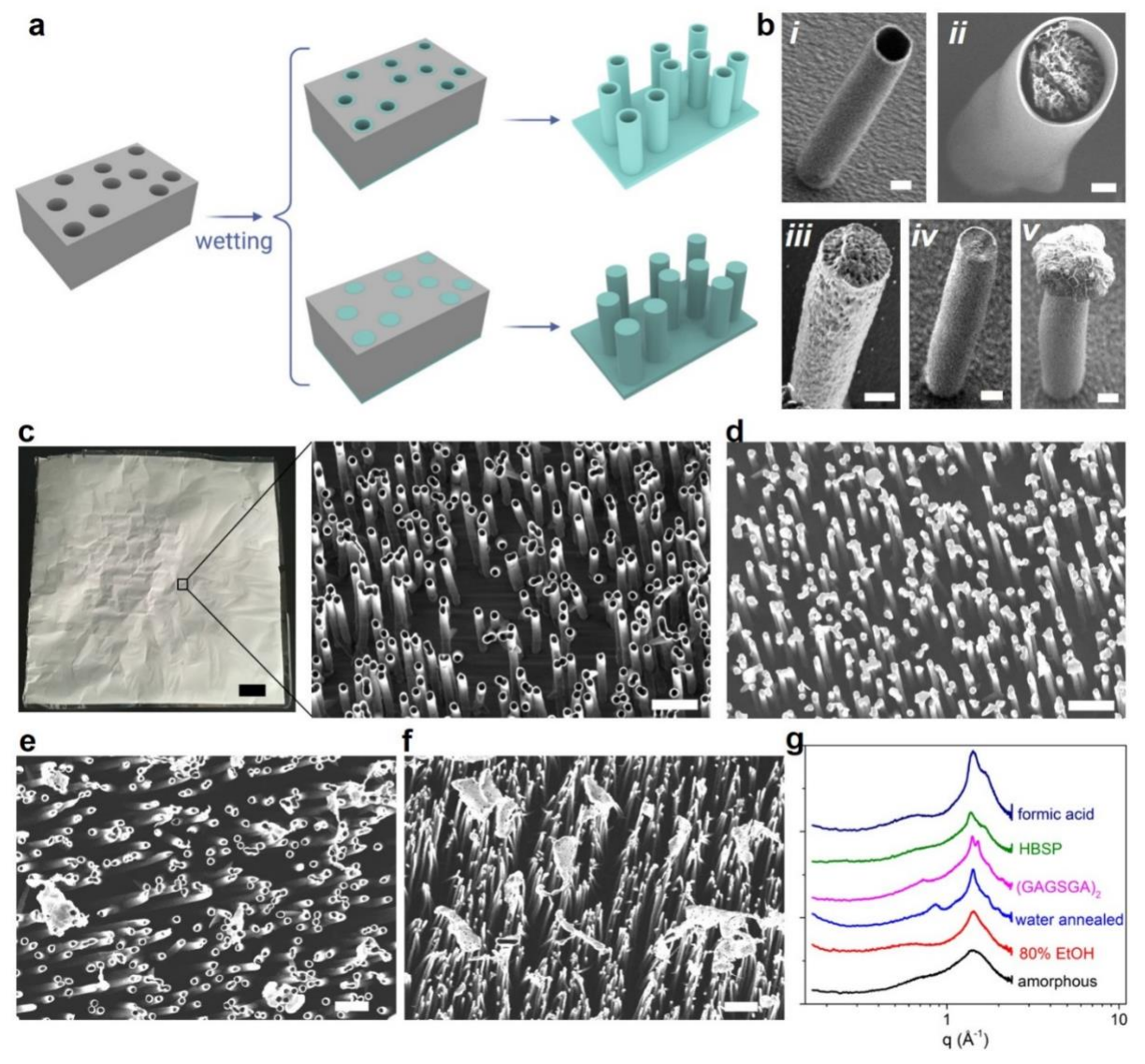


Figure 1. Fabrication of silk nanotube/pillar array through wetting of nanoporous polycarbonate (PC) membranes. **a,** Schematic of the template wetting approach to generate either silk nanotube or nanopillar array through different wetting behaviors. **b,** SEM images of (i) silk nanotube, (ii) silk nanotube-CaCO₃ composite, (iii) porous nanopillar, (iv) solid nanopillar, and (v) mushroom-shaped pillar, obtained from the templated assembly process shown in **a.** Scale bars, 500 nm. **c,** A 20×20 cm² free-standing silk nanotube array templated from PC membranes of 1 μm pore size and its microscopic view under SEM. Scale bars, 2 cm (left) and 5 μm (right). **d,** An array of silk nanopillars templated from PC membranes of 1 μm pore size. Scale bar, 5 μm. **e,** An array of silk nanotubes of tube diameter 400 nm. Scale bar, 2 μm. **f,** An array of silk nanotubes of tube diameter 100 nm obtained by critical point drying. Scale bar, 2 μm. **g,** WAXS spectra of silk nanotube arrays made of different silk polymorphs.

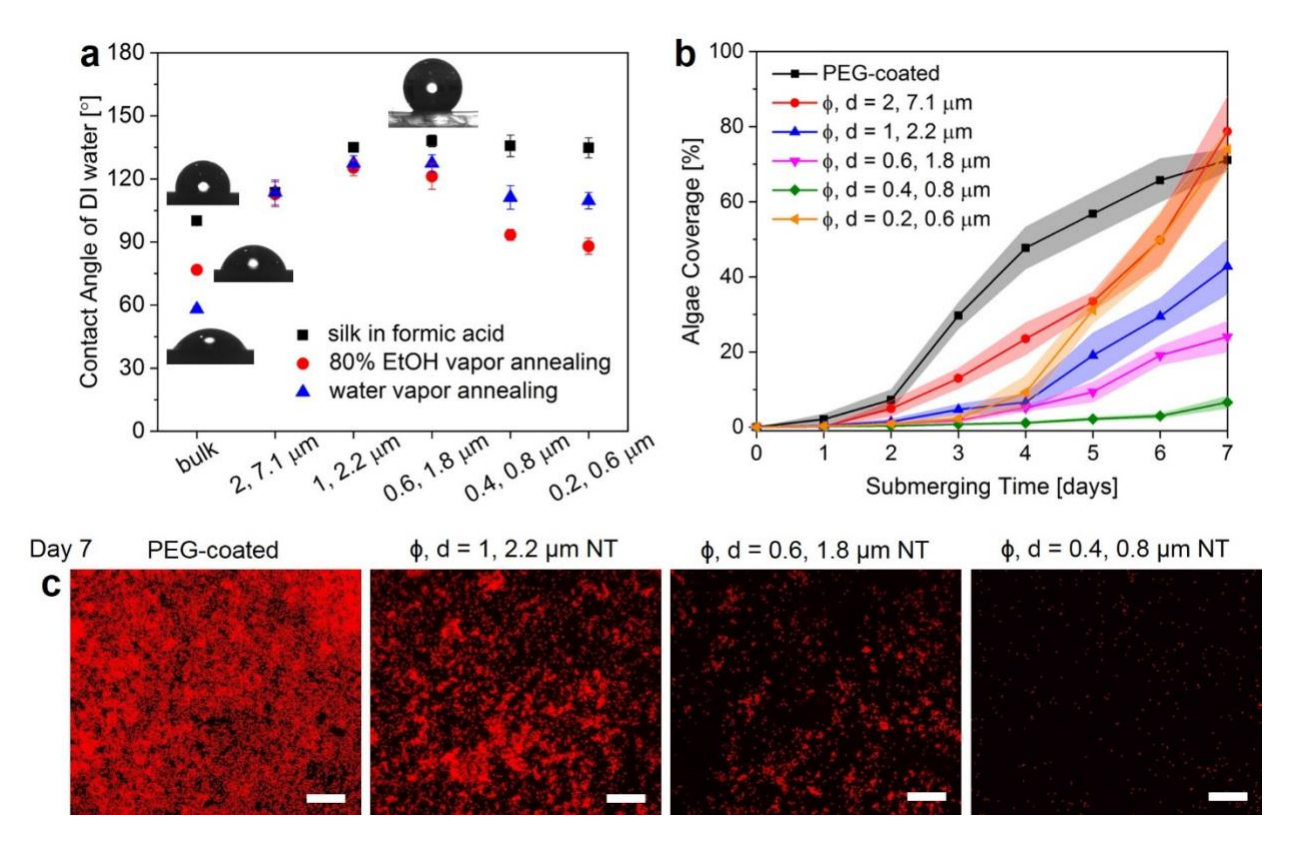


Figure 2. Hydrophobicity and anti-fouling of silk nanotube arrays. **a,** Static contact angles of water on bulk silk membranes and silk nanotube arrays of different tube diameter ϕ and inter-tube distance d, made from three types of silk (i.e. silk dried from silk-FA suspension, 80% EtOH-annealed silk, and water-annealed silk). **b,** Area fraction of algae coverage on PEG-coated and silk nanotube-coated glass coverslips over time. **c,** Fluorescence microscopy images showing algae distribution and coverage on PEG-coated and silk nanotube-coated glass coverslips after being incubated in the algae culture for 7 days. Scale bars, 200 μ m.

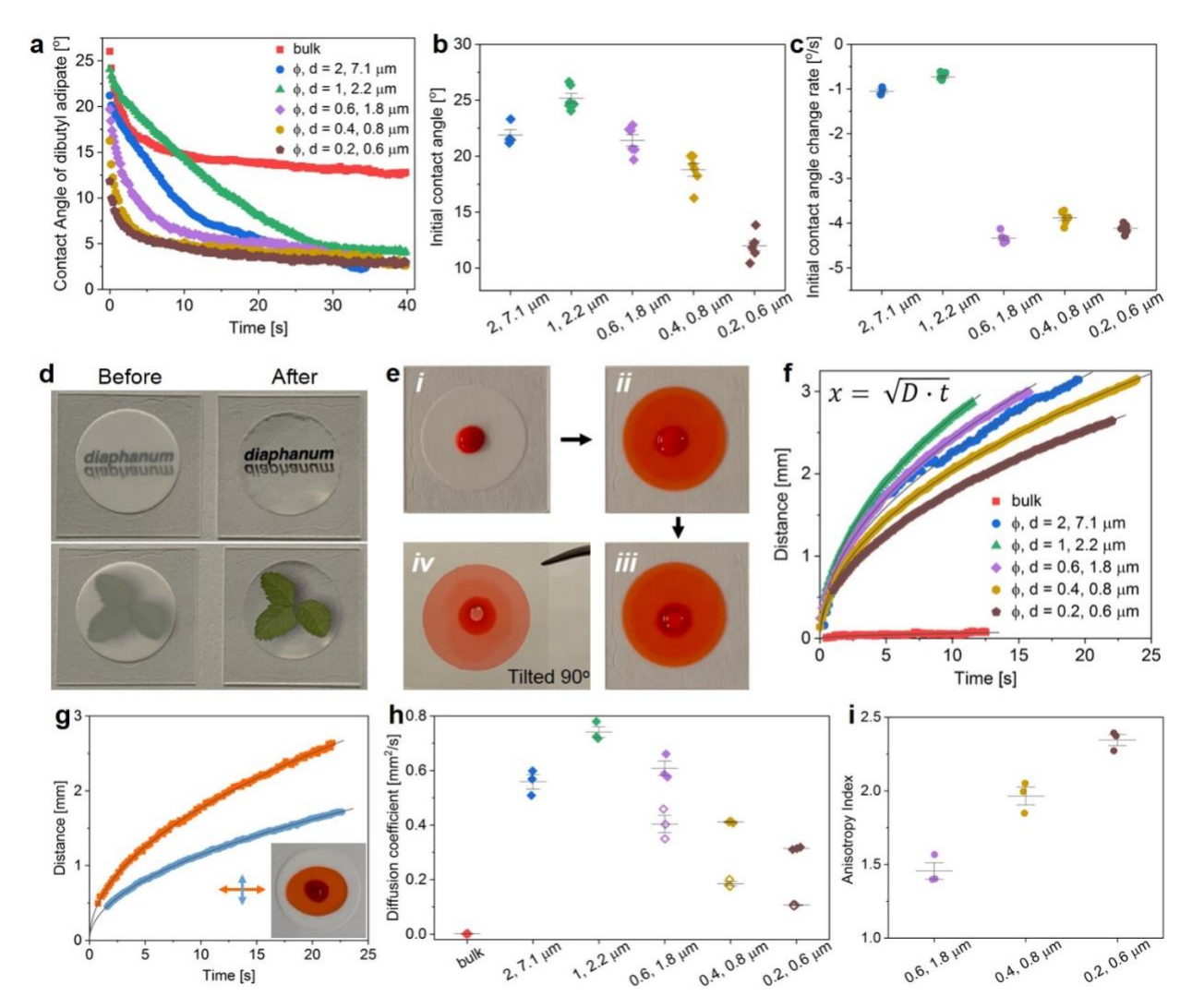


Figure 3. Superoleophilicity and oil extraction from oil-water emulsions by silk nanotube arrays. **a**, Dynamic contact angles of dibutyl adipate (DA) on bulk silk membranes and silk nanotube arrays of different tube diameter φ and inter-tube distance d. **b**, Initial contact angle of DA on silk nanotube arrays of different (φ, d) at t=0. **c**, Initial contact angle change rates obtained by linear fitting of the initial data points in **a**. **d**, Silk nanotube array of φ, d = 0.2, 0.6 μm before and after being infiltrated by an oil that has a refractive index (RI) of 1.55 which is very similar to the RI of silk. **e**, DA diffusion from the DA-water emulsion deposited on top of a silk nanotube array across the entire silk nanotube array. **f**, Plots of DA diffusion distance from the center of the DA-water emulsion as a function of time, and their fitting by equation $\mathbf{x} = \sqrt{\mathbf{D} \cdot \mathbf{t}}$, where D is the diffusion coefficient. **g**, Anisotropic DA diffusion over a silk nanotube array of φ, d = 0.2, 0.6 μm. **h**, Diffusion coefficients extracted from the data fitting in **f** and **g** (n=3). **i**, Anisotropy index of oil diffusion (defined by $D_{\text{max}}/D_{\text{min}}$) calculated from the data in **h**.

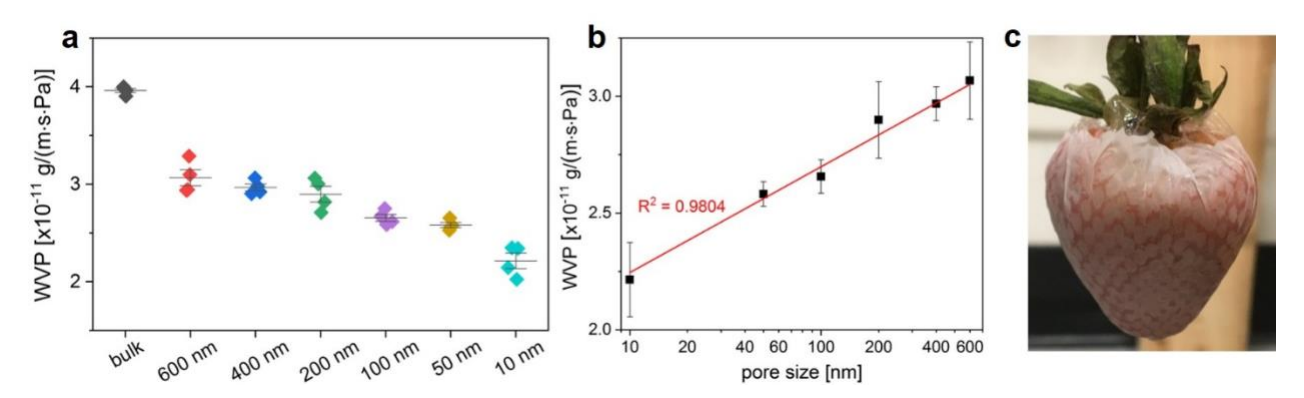


Figure 4. Water vapor permeability (WVP) of silk nanotube membranes. **a,** WVP values of bulk silk membranes and nanostructured silk membranes of different nominal pore sizes (NPS). **b,** WVP values plotted against the NPS of silk nanotube membranes on a log scale, showing a linear decrease of WVP with respect to the logarithm of NPS. **c,** Photography of a strawberry coated with a silk nanotube membrane.

ASSOCIATED CONTENT

Supporting Information. The following files are available free of charge.

Experimental details on materials preparation, fabrication and characterization, and ten supporting figures (PDF)

A movie showing the wetting process of a silk nanotube array by dibutyl adipate (DA) (MP4) A movie showing the extraction of dyed DA from DA-water emulsions by a silk nanotube array (MOV)

AUTHOR INFORMATION

Corresponding Author

* Benedetto Marelli – Department of Civil and Environmental Engineering, Massachusetts Institute of Technology, Cambridge, MA 02139, USA; Email: bmarelli@mit.edu

Author Contributions

H.S. and B.M. conceived the idea and designed the research. H.S. performed the experiments, analyzed the experimental data, and wrote the first draft of the manuscript. All authors contributed to the preparation of the final manuscript.

Funding Sources

Office of Naval Research (Awards N000142112402 and N000141912317) and National Science Foundation (Award CMMI-1752172).

Notes

H.S. and B.M. are inventors on a patent application (Serial No. 63/481,633) filed by Massachusetts Institute of Technology that covers the technology reported in this manuscript. The authors declare no other competing interests.

ACKNOWLEDGMENT

This work was partially supported by the Office of Naval Research (Awards N000142112402 and N000141912317) and the National Science Foundation (Award CMMI-1752172). B.M. acknowledges a Paul M. Cook Career Development Professorship and a Singapore Research Professorship. The authors gratefully acknowledge the Materials Research Laboratory (MRL),

MIT.nano, Institute for Soldier Nanotechnologies (ISN), and Nanostructures Laboratory (NSL), all at MIT, for access to the characterization instruments.

REFERENCES

- (1) Iijima, S. Helical Microtubules of Graphitic Carbon. *Nature* **1991**, *354* (6348), 56–58.
- (2) Schnorr, J. M.; Swager, T. M. Emerging Applications of Carbon Nanotubes. *Chem. Mater.* **2011**, *23* (3), 646–657.
- (3) Bianco, A.; Kostarelos, K.; Prato, M. Applications of Carbon Nanotubes in Drug Delivery. *Curr. Opin. Chem. Biol.* **2005**, *9* (6), 674–679.
- (4) Hinds, B. J.; Chopra, N.; Rantell, T.; Andrews, R.; Gavalas, V.; Bachas, L. G. Aligned Multiwalled Carbon Nanotube Membranes. *Science* (80-.). **2004**, 303 (5654), 62–65.
- (5) Sun, M.; Boo, C.; Shi, W.; Rolf, J.; Shaulsky, E.; Cheng, W.; Plata, D. L.; Qu, J.; Elimelech, M. Engineering Carbon Nanotube Forest Superstructure for Robust Thermal Desalination Membranes. *Adv. Funct. Mater.* 2019, 29 (36), 1903125.
- (6) Sun, Y.; Xia, Y. Multiple-walled Nanotubes Made of Metals. *Adv. Mater.* **2004**, *16* (3), 264–268.
- (7) Liang, H.; Liu, S.; Yu, S. Controlled Synthesis of One-dimensional Inorganic Nanostructures Using Pre-existing One-dimensional Nanostructures as Templates. *Adv. Mater.* **2010**, *22* (35), 3925–3937.
- (8) Goldberger, J.; He, R.; Zhang, Y.; Lee, S.; Yan, H.; Choi, H.-J.; Yang, P. Single-Crystal Gallium Nitride Nanotubes. *Nature* **2003**, *422* (6932), 599–602.
- (9) Steinhart, M.; Wendorff, J. H.; Greiner, A.; Wehrspohn, R. B.; Nielsch, K.; Schilling, J.; Choi, J.; Gosele, U. Polymer Nanotubes by Wetting of Ordered Porous Templates. *Science* (80-.). **2002**, 296 (5575), 1997.
- (10) Jin, M.; Feng, X.; Feng, L.; Sun, T.; Zhai, J.; Li, T.; Jiang, L. Superhydrophobic Aligned Polystyrene Nanotube Films with High Adhesive Force. *Adv. Mater.* **2005**, *17* (16), 1977–1981.
- (11) Adler-Abramovich, L.; Aronov, D.; Beker, P.; Yevnin, M.; Stempler, S.; Buzhansky, L.; Rosenman, G.; Gazit, E. Self-Assembled Arrays of Peptide Nanotubes by Vapour Deposition. *Nat. Nanotechnol.* 2009, 4 (12), 849–854.

- https://doi.org/10.1038/Nnano.2009.298.
- (12) Steinhart, M.; Wehrspohn, R. B.; Gösele, U.; Wendorff, J. H. Nanotubes by Template Wetting: A Modular Assembly System. *Angew. Chemie Int. Ed.* **2004**, *43* (11), 1334–1344.
- (13) Shimizu, T.; Masuda, M.; Minamikawa, H. Supramolecular Nanotube Architectures Based on Amphiphilic Molecules. *Chem. Rev.* **2005**, *105* (4), 1401–1444.
- (14) Zhou, Y.; Shimizu, T. Lipid Nanotubes: A Unique Template to Create Diverse One-Dimensional Nanostructures. *Chem. Mater.* **2008**, *20* (3), 625–633.
- (15) Hamley, I. W. Peptide Nanotubes. Angew. Chemie Int. Ed. 2014, 53 (27), 6866–6881.
- (16) Guerette, P. A.; Hoon, S.; Seow, Y.; Raida, M.; Masic, A.; Wong, F. T.; Ho, V. H. B.; Kong, K. W.; Demirel, M. C.; Pena-Francesch, A. Accelerating the Design of Biomimetic Materials by Integrating RNA-Seq with Proteomics and Materials Science. *Nat. Biotechnol.* 2013, 31 (10), 908–915.
- (17) Cantaert, B.; Ding, D.; Rieu, C.; Petrone, L.; Hoon, S.; Kock, K. H.; Miserez, A. Stable Formation of Gold Nanoparticles onto Redox-Active Solid Biosubstrates Made of Squid Suckerin Proteins. *Macromol. Rapid Commun.* **2015**, *36* (21), 1877–1883.
- (18) Komatsu, T.; Qu, X.; Ihara, H.; Fujihara, M.; Azuma, H.; Ikeda, H. Virus Trap in Human Serum Albumin Nanotube. *J. Am. Chem. Soc.* **2011**, *133* (10), 3246–3248.
- (19) Komatsu, T. Protein-Based Nanotubes for Biomedical Applications. *Nanoscale* **2012**, *4* (6), 1910–1918.
- (20) Cheng, C.; Shao, Z. Z.; Vollrath, F. Silk Fibroin-Regulated Crystallization of Calcium Carbonate. *Adv. Funct. Mater.* **2008**, *18* (15), 2172–2179. https://doi.org/10.1002/adfm.200701130.
- (21) Lopes, J. H.; Guilhou, M.; Marelli, B.; Omenetto, F. G.; Kaplan, D. L.; Barralet, J. E.; Merle,
 G. Silk Fibroin Hydroxyapatite Composite Thermal Stabilisation of Carbonic Anhydrase.
 J. Mater. Chem. A 2015, 3 (38), 19282–19287.
- (22) Partlow, B. P.; Hanna, C. W.; Rnjak-Kovacina, J.; Moreau, J. E.; Applegate, M. B.; Burke, K. A.; Marelli, B.; Mitropoulos, A. N.; Omenetto, F. G.; Kaplan, D. L. Highly Tunable Elastomeric Silk Biomaterials. *Adv. Funct. Mater.* **2014**, *24* (29), 4615–4624. https://doi.org/10.1002/adfm.201400526.
- (23) Tseng, P.; Napier, B.; Zhao, S. W.; Mitropoulos, A. N.; Applegate, M. B.; Marelli, B.; Kaplan, D. L.; Omenetto, F. G. Directed Assembly of Bio-Inspired Hierarchical Materials

- with Controlled Nanofibrillar Architectures. *Nat. Nanotechnol.* **2017**, *12* (5), 474–480. https://doi.org/10.1038/Nnano.2017.4.
- (24) Zhang, F.; You, X.; Dou, H.; Liu, Z.; Zuo, B.; Zhang, X. Facile Fabrication of Robust Silk Nanofibril Films via Direct Dissolution of Silk in CaCl2–Formic Acid Solution. *ACS Appl. Mater. Interfaces* **2015**, *7* (5), 3352–3361.
- (25) Jiang, J. J.; Zhang, S. Q.; Qian, Z. G.; Qin, N.; Song, W. W.; Sun, L.; Zhou, Z. T.; Shi, Z. F.; Chen, L.; Li, X. X.; Mao, Y.; Kaplan, D. L.; Corder, S. N. G.; Chen, X. Z.; Liu, M. K.; Omenetto, F. G.; Xia, X. X.; Tao, T. H. Protein Bricks: 2D and 3D Bio-Nanostructures with Shape and Function on Demand. *Adv. Mater.* 2018, 30 (20). https://doi.org/ARTN 170591910.1002/adma.201705919.
- (26) Kim, S.; Marelli, B.; Brenckle, M. A.; Mitropoulos, A. N.; Gil, E. S.; Tsioris, K.; Tao, H.; Kaplan, D. L.; Omenetto, F. G. All-Water-Based Electron-Beam Lithography Using Silk as a Resist. *Nat. Nanotechnol.* **2014**, *9* (4), 306–310. https://doi.org/10.1038/Nnano.2014.47.
- (27) Jin, H.; Park, J.; Karageorgiou, V.; Kim, U.; Valluzzi, R.; Cebe, P.; Kaplan, D. L. Waterstable Silk Films with Reduced B-sheet Content. *Adv. Funct. Mater.* **2005**, *15* (8), 1241–1247.
- (28) Sun, H.; Marelli, B. Polypeptide Templating for Designer Hierarchical Materials. *Nat. Commun.* **2020**, *11* (1), 1–13. https://doi.org/10.1038/s41467-019-14257-0.
- (29) Feng, L.; Li, S.; Li, Y.; Li, H.; Zhang, L.; Zhai, J.; Song, Y.; Liu, B.; Jiang, L.; Zhu, D. Super-hydrophobic Surfaces: From Natural to Artificial. *Adv. Mater.* **2002**, *14* (24), 1857–1860.
- (30) Cassie, A. B. D.; Baxter, Sjt. Wettability of Porous Surfaces. *Trans. Faraday Soc.* **1944**, *40*, 546–551.
- (31) Sun, T.; Tan, H.; Han, D.; Fu, Q.; Jiang, L. No Platelet Can Adhere—Largely Improved Blood Compatibility on Nanostructured Superhydrophobic Surfaces. *Small* **2005**, *1* (10), 959–963.
- (32) Wang, J.; Lee, S.; Bielinski, A. R.; Meyer, K. A.; Dhyani, A.; Ortiz-Ortiz, A. M.; Tuteja, A.; Dasgupta, N. P. Rational Design of Transparent Nanowire Architectures with Tunable Geometries for Preventing Marine Fouling. Adv. Mater. Interfaces 2020, 7 (17), 2000672.
- (33) Zhang, L.; Shi, X.; Sun, M.; Porter, C. J.; Zhou, X.; Elimelech, M. Precisely Engineered Photoreactive Titanium Nanoarray Coating to Mitigate Biofouling in Ultrafiltration. *ACS*

- Appl. Mater. Interfaces 2021, 13 (8), 9975–9984.
- (34) Marcati, A.; Ursu, A. V.; Laroche, C.; Soanen, N.; Marchal, L.; Jubeau, S.; Djelveh, G.; Michaud, P. Extraction and Fractionation of Polysaccharides and B-Phycoerythrin from the Microalga Porphyridium Cruentum by Membrane Technology. *Algal Res.* 2014, 5, 258–263.
- (35) Krishnan, S.; Weinman, C. J.; Ober, C. K. Advances in Polymers for Anti-Biofouling Surfaces. *J. Mater. Chem.* **2008**, *18* (29), 3405–3413.
- (36) Feng, X. J.; Jiang, L. Design and Creation of Superwetting/Antiwetting Surfaces. *Adv. Mater.* **2006**, *18* (23), 3063–3078.
- (37) Zhang, J.; Du, S.; Kafi, A.; Fox, B.; Li, J. L.; Liu, X. Y.; Rajkhowa, R.; Wang, X. G. Surface Energy of Silk Fibroin and Mechanical Properties of Silk Cocoon Composites. *Rsc Adv.* 2015, 5 (2), 1640–1647.
- (38) Gore, P. M.; Naebe, M.; Wang, X.; Kandasubramanian, B. Silk Fibres Exhibiting Biodegradability & Superhydrophobicity for Recovery of Petroleum Oils from Oily Wastewater. *J. Hazard. Mater.* **2020**, *389*, 121823.
- (39) Parker, S. T.; Domachuk, P.; Amsden, J.; Bressner, J.; Lewis, J. A.; Kaplan, D. L.; Omenetto, F. G. Biocompatible Silk Printed Optical Waveguides. *Adv. Mater.* **2009**, *21* (23), 2411–2415.
- (40) Zhang, W.; Shi, Z.; Zhang, F.; Liu, X.; Jin, J.; Jiang, L. Superhydrophobic and Superoleophilic PVDF Membranes for Effective Separation of Water-in-oil Emulsions with High Flux. *Adv. Mater.* **2013**, *25* (14), 2071–2076.
- (41) Li, Z.; Wang, B.; Qin, X.; Wang, Y.; Liu, C.; Shao, Q.; Wang, N.; Zhang, J.; Wang, Z.; Shen, C. Superhydrophobic/Superoleophilic Polycarbonate/Carbon Nanotubes Porous Monolith for Selective Oil Adsorption from Water. ACS Sustain. Chem. Eng. 2018, 6 (11), 13747–13755.
- (42) Berg, H. C. Random Walks in Biology; Princeton University Press, 2018; pp 5–16. https://doi.org/doi:10.1515/9781400820023-004.
- (43) Marelli, B.; Brenckle, M. A.; Kaplan, D. L.; Omenetto, F. G. Silk Fibroin as Edible Coating for Perishable Food Preservation. *Sci. Rep.* **2016**, *6*. https://doi.org/ARTN 2526310.1038/srep25263.
- (44) Ruggeri, E.; Kim, D.; Cao, Y.; Farè, S.; De Nardo, L.; Marelli, B. A Multilayered Edible

- Coating to Extend Produce Shelf Life. *ACS Sustain. Chem. Eng.* **2020**, *8* (38), 14312–14321. https://doi.org/10.1021/acssuschemeng.0c03365.
- (45) Yoon, D.; Lee, C.; Yun, J.; Jeon, W.; Cha, B. J.; Baik, S. Enhanced Condensation, Agglomeration, and Rejection of Water Vapor by Superhydrophobic Aligned Multiwalled Carbon Nanotube Membranes. *ACS Nano* **2012**, *6* (7), 5980–5987.

TOC Graphic

